Optimization of power compression and stability of relativistic and ponderomotive self-channeling of 248 nm laser pulses in underdense plasmas

J. Davis,[1] A. B. Borisov,[2] and C. K. Rhodes[2,3,4,5]
[1]*Plasma Physics Division, Naval Research Laboratory, 4555 Overlook Avenue SW, Washington, D.C. 20375, USA*
[2]*Laboratory for X-Ray Microimaging and Bioinformatics, Department of Physics M/C 273, University of Illinois at Chicago, 845 West Taylor Street, Chicago, Illinois 60607-7059, USA*
[3]*Department of Bioengineering, M/C 063, University of Illinois at Chicago, 851 South Morgan Street, Chicago, Illinois 60607-7052, USA*
[4]*Department of Computer Science, M/C 102, University of Illinois at Chicago, 851 South Morgan Street, Chicago, Illinois 60607-7042, USA*
[5]*Department of Electrical and Computer Engineering, M/C 154, University of Illinois at Chicago, 851 South Morgan Street, Chicago, Illinois 60607-7053, USA*
(Received 18 June 2004; published 20 December 2004)

The controlled formation in an underdense plasma of stable multi-PW relativistic micrometer-scale channels, which conduct a confined power at 248 nm exceeding 10^4 critical powers and establish a peak channel intensity of $\sim 10^{23}$ W/cm^2, can be achieved with the use of an appropriate gradient in the electron density in the initial launching phase of the confined propagation. This mode of channel formation optimizes both the power compression and the stability by smoothing the transition from the incident spatial profile to that associated with the lowest channel eigenmode, the dynamically robust structure that governs the confined propagation. A chief outcome is the ability to stably conduct coherent energy at fluences greater than 10^9 J/cm^2.

DOI: 10.1103/PhysRevE.70.066406 PACS number(s): 52.35.Mw, 52.38.Hb

I. INTRODUCTION

The phenomenon of self-focusing of powerful laser pulses in nonlinear media [1–4] has been one of the key factors that (1) historically triggered rapid progress in theoretical nonlinear optics and (2) drove the development of high peak power laser systems. Following an initial theoretical phase that included detailed numerical assessments [5–8], the predicted self-channeling property of the relativistic/charge-displacement mechanism was initially experimentally demonstrated at an ultraviolet wavelength (248 nm) in Ref. [9]. Subsequently, in a second round of experimental studies of this high intensity mode of confined propagation, the observation of relativistic channels with lengths exceeding 100 Rayleigh ranges was reported [10]. At the present time, more than a decade after the first experimental observation [9], the relativistic and ponderomotive mechanism of self-channeling stands as the first rank method for the *controlled* power compression of high intensity laser pulses in plasmas. Major applications associated with these relativistic channels include (a) the generation of coherent x rays, (b) particle acceleration, and (c) the fast ignition of fusion targets.

A chief issue facing any mode of power compression in plasmas is the stability of the compressed configuration. For the relativistic mechanism under consideration, the principal vulnerability is the potential for transverse instability of the self-channeled propagation, a process that destroys the power compression through the uncontrolled development of multiple peripheral filaments. This form of transverse instability was first demonstrated both theoretically [11] and experimentally [12,13] in the case of Kerr self-focusing. In contrast to the Kerr case, studies of the stability of propagation for the relativistic charge-displacement mechanism in uniform underdense plasmas [14–17] have revealed the existence of large stable zones of confined propagation. The basis of the finding is the existence of an eigenmode that governs the propagation and confers on it a robust stability sufficiently strong to damp even large levels of azimuthal perturbation [14]. The physical origin of this stability is the energetics of the charge displacement. Accordingly, for the first time, the relativistic charge-displacement mechanism brought into alliance two prized attributes in the world of confined plasmas, (i) exceptionally high power density ($\sim 10^{20}$ W/cm^3) and (ii) a state of propagation exhibiting unconditional stability.

Analyses of the stability of the relativistic and ponderomotive mechanism have distinguished [14–17] three major modes of self-channeling action. They are (1) the unconditionally stable mode that leads directly to the formation of a single stable ultrapowerful channel, (2) the fully unstable mode, which is characterized by the uncontrolled development of multiple peripheral filaments each carrying a power on the order of the critical power P_{cr}, and (3) the bifurcation mode of the self-channeling, an intermediate situation of limited instability that occurs when the transverse instability leads to the splitting of the beam into two or a relatively small number of powerful channels each possessing a power P_{ch} considerably in excess of a critical power (e.g., $P_{ch} \gg P_{cr}$).

In the high power regime ($P \gg P_{cr}$), the development of stable channels is decisively influenced by the conditions of channel initiation. For example, when $P \gg P_{cr}$ and the radius of the incident beam is considerably larger than the radius of the eigenmode of the relativistic channel, highly unstable filamentation is the dominant mode of propagation [14]. Importantly, it has been established, both numerically [15,16] and experimentally [17], that these unstable modes of propa-

gation can be transformed into corresponding stable modes with proper control of the gradient in the electron density during the initial stage of channel formation. The growth of the instability can be *dynamically* blocked. Specifically, the use of a longitudinal variation in the medium restores the stable flow of energy to the eigenmode by enabling the incident pulse to be matched *adiabatically* to the spatial character of the eigenmode. Moreover, the length of the initial zone that possesses the appropriate gradient in the electron density profile can be relatively short, on the order of the Rayleigh range. Typically, this distance is much shorter than the characteristic length for dissipation of the laser pulse energy in cold underdense plasmas. Therefore, the energy losses are negligible for stable channel formation in the initial launching phase of the self-channeling; these losses only affect the total length of the channeled propagation.

The computational results discussed below for radiation at a wavelength of 248 nm demonstrate that this technique can be used to optimize the formation and control of stable channels in underdense plasmas in the multi-PW regime. These channels conduct a power exceeding 10^4 critical powers and generate peak channel intensities in the $\sim 10^{23}$ W/cm^2 range. We note that the suppression of the transverse instabilities for the laser pulses with the peak intensity in the 10^{23} W/cm^2 range has also been demonstrated numerically in recent three-dimensional particle-in-cell (PIC) simulations [18] of ion acceleration with ultrapowerful laser pulses penetrating high density plasmas (see Ref. [19] for a review of PIC simulations of the relativistic self-channeling).

II. SELF-CHANNELING MODEL AND ANALYTICAL ANALYSIS

The stability analysis of the relativistic and ponderomotive mechanism of self-channeling is founded on a basic physical model [7,8] that involves two chief dimensionless parameters (η, ρ_0). They represent the normalized power η and normalized radius ρ_0 of the incident beam and are defined by

$$\eta = P_0/P_{\mathrm{cr}} \quad \text{and} \quad \rho_0 = r_0\omega_{p,0}/c. \tag{1}$$

In Eq. (1), P_0 and r_0, respectively, denote the peak power and the radius of the incident beam and P_{cr} represents the critical power [7,8] for relativistic and ponderomotive self-channeling given [8] by

$$P_{\mathrm{cr}} = (m_{e,0}^2c^5/e^2)\int_0^\infty g_0^2(\rho)\rho\, d\rho(\omega/\omega_{p,0})^2 = 1.6198\times 10^{10}(\omega/\omega_{p,0})^2 W, \tag{2}$$

in which $m_{e,0}, c$, and e have their standard identifications, $g_0(\rho)$ is the Townes mode [2], ω is the angular frequency of the laser radiation, and $\omega_{p,0}$ represents the angular plasma frequency

$$\omega_{p,0} = (4\pi e^2\, N_{e,0}/m_{e,0})^{1/2}. \tag{3}$$

The process of the self-channeling can be described as the stabilization of the transverse beam profile near one of the z-independent modes of propagation identified [8,14] as the lowest eigenmodes $U_{s,0}(\rho)$ of the governing nonlinear Schrödinger equation. The index s, which falls in the interval $0<s<1$, is associated with the normalized power η of the eigenmodes. The quantity $\rho=r\omega_{p,0}/c$ represents the normalized transverse variable, where r is the transverse spatial coordinate. The normalized radius $\rho_{e,0}$ of the eigenmodes $U_{s,0}(\rho)$ can be defined as

$$\rho_{e,0} \equiv \left(2\int_0^\infty U_{s,0}^2(\rho)\rho\, d\rho/U_{s,0}^2(0)\right)^{1/2}. \tag{4}$$

Since the eigenmodes $U_{s,0}(\rho)$ represent the normalized transverse field profiles of the relativistic channels, a specific eigenmode curve $\rho_{e,0}(\eta)$ identifies the normalized radius of the relativistic channel as a function of the normalized power η trapped in the channel. Thus, the radius of the channel r_{ch} can be expressed as

$$r_{\mathrm{ch}} = \frac{c\rho_{e,0}}{\omega_p} \tag{5}$$

and

$$r_{\mathrm{ch}} = \frac{\rho_{e,0}}{2\pi}\lambda\ (N_e/N_{\mathrm{cr}})^{-1/2}. \tag{6}$$

Since $\rho_{e,0}$ varies slowly [14] for $\eta>1.5$, we conclude that the radius of the relativistic channel scales approximately as

$$r_{\mathrm{ch}} \sim N_e^{-1/2}. \tag{7}$$

Accordingly, from Eqs. (4) and (6), the peak laser intensity in the relativistic channel I_{ch} can be expressed as

$$I_{\mathrm{ch}} = \frac{4\pi}{\rho_{e,0}^2}\frac{N_e}{N_{\mathrm{cr}}}P_{\mathrm{ch}}\lambda^{-2}, \tag{8}$$

in which P_{ch} represents the power trapped in the channel. Again, since $\rho_{e,0}$ varies slowly [14] for $\eta>1.5$, the peak intensity in relativistic channels scales as

$$I_{\mathrm{ch}} \sim \frac{N_e}{N_{\mathrm{cr}}}P_{\mathrm{ch}}\lambda^{-2}. \tag{9}$$

For a constant ratio of N_e/N_{cr}, the simple scaling relations

$$r_{\mathrm{ch}} \sim \lambda \quad \text{and} \quad I_{\mathrm{ch}} \sim P_{\mathrm{ch}}\lambda^{-2} \tag{10}$$

follow from Eqs. (6) and (9).

The propagation of ultrapowerful $(\eta=P_0/P_{\mathrm{cr}}\gg 1)$ laser pulses, under conditions for which the initial radius of the beam r_0 is much larger than the radius of the channel ($r_0\gg r_{\mathrm{ch}}$, or $\rho_0\gg\rho_{e,0}$), is generally explosively unstable. The canonical outcome is a rapid and uncontrolled formation of multiple peripheral filaments; the channel disintegrates. In order to restore channel formation and stable propagation, and likewise optimize the efficiency of the power compression, an appropriate spatial match between the radius of the incident beam and the characteristic radius of the channel has to be attained, namely,

$$r_0 \sim r_{\mathrm{ch}} \quad \text{or} \quad \rho_0 \sim \rho_{e,0}. \tag{11}$$

Since $r_{\mathrm{ch}}\sim N_c^{-1/2}$, the condition specified by Eq. (11) can be

achieved *dynamically* through the adjustment of the local electron density N_e, with the provision of a suitable longitudinal gradient in that quantity.

III. RESULTS OF NUMERICAL MODELING

A. Multiterawatt regime

The chief physical parameters of the numerical stability analysis conducted in the present study are (1) the incident peak power, (2) the radius of the incident laser beam, (3) the level of the azimuthal perturbations of the incident transverse intensity distribution, (4) the length of the initial stage of channel formation involving the longitudinal gradient in the electron density, and (5) the level and spatial distribution of the electron density profile in the initial region in which the channels characteristic of the eigenmode are developed.

The stability analysis was performed for azimuthally perturbed Gaussian beams specified by an incident transverse amplitude distribution given by

$$U_0(r,\phi) = I_0^{1/2} \exp[-0.5(r/r_0)^2]\Big(1 + (r/r_0)^4 \sum \varepsilon_q \cos(q\phi)\Big). \tag{12}$$

The strength of the azimuthal perturbations in Eq. (12) is characterized by the parameter δ_{pert} defined through

$$\delta_{\text{pert}} = \max |I_0(r,\phi_1) - I_0(r,\phi_2)|/I_0. \tag{13}$$

For $\varepsilon_q = 0.01$ ($q = 1-4$) in Eq. (12) , $\delta_{\text{pert}} = 0.063$, and correspondingly for $\varepsilon_q = 0.05$ ($q = 1-4$) $\delta_{\text{pert}} = 0.393$.

In the results presented in the sequence of figures following below, the transverse coordinates (x,y) are normalized by the radius of the incident transverse intensity profile r_0 [see Eq. (12)] and the longitudinal coordinate z is normalized by the Rayleigh length L_R. In the case of axisymmetric Gaussian beams, we have $L_R = \pi w_0^2/\lambda$, where w_0 is the waist of the incident transverse amplitude profile. Further, since $w_0 = \sqrt{2} r_0$ [see Eq. (12)], we have $L_R = 2\pi r_0^2/\lambda$.

Figure 1 illustrates the classic behavior of a highly unstable mode. A smooth beam profile incident on an initially uniform plasma results in the catastrophic formation of multiple peripheral filaments. The incident transverse intensity distribution is presented in Fig. 1(a). The corresponding level of the azimuthal perturbation of the incident transverse intensity profile is $\delta_{\text{pert}} = 0.063$. The chief laser beam, and plasma parameters in this case are $\lambda = 248$ nm, $P_0 = 39$ TW, $r_0 = 10$ μm, $I_0 = 1.2 \times 10^{19}$ W/cm^2, $\varepsilon_q \equiv 0.01$ ($q = 1-4$), $\delta_{\text{pert}} = 0.063$, and $N_{e,0} = 3.8 \times 10^{20}$ cm^{-3}. The normalized power and beam radius in this case are $\eta = P_0/P_{\text{cr}} \cong 50$ and $\rho_0 \cong 37$. Figure 1(b) depicts the transverse profile consisting of the multiple filaments that evolve in the process of the highly unstable propagation.

The restoration of both stable propagation of the channel and efficient power compression can be achieved through the use of the two-step self-channeling mechanism introduced above (see Fig. 2). The first stage, which initiates the stable channel formation, involves an exponential longitudinal gradient in the electron density profile defined by $N_{e,0}(z) = N_{e,0}(0)\exp(\alpha z)$. In the specific example considered, we have $N_{e,0}(0) = 1.9 \times 10^{19}$ cm^{-3}, $N_{e,0,\max} = 3.8 \times 10^{20}$ cm^{-3}, and $z_{\max} = 3.16 L_R$ ($\alpha = 0.949$), where $z_{\max}$ is the length of the first stage and the point at which electron density N_e reaches the maximum value $N_{e,0,\max}$. All of the parameters associated with the propagation are otherwise the same as those used in the previous case above (see Fig. 1). Accordingly, the transverse incident intensity profile is identical to that presented in Fig. 1(a). The corresponding development of a stable channel that demonstrates the efficacy of the two-step process involving the exponential longitudinal electron density profile is shown in Fig. 2. It is evident that the highly unstable structure with multiple filaments given in Fig. 1(b) has been transformed into a single stable channel.

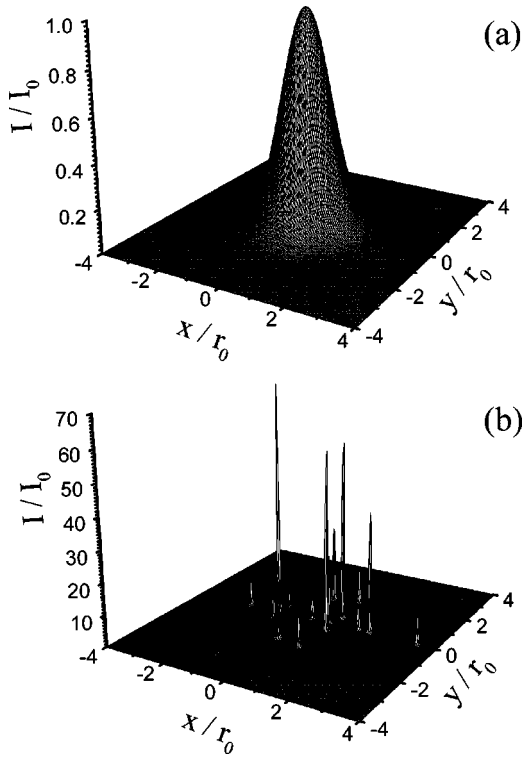

FIG. 1. Highly unstable relativistic and ponderomotive self-channeling of an azimuthally perturbed multi-TW laser pulse in an initially uniform underdense plasma. The laser and plasma parameters are $\lambda = 248$ nm, $P_0 = 39$ TW, $r_0 = 10$ μm, $I_0 = 1.2 \times 10^{19}$ W/cm^2, and $N_{e,0} = 3.8 \times 10^{20}$ cm^{-3}. The normalized power and beam radius in this case are, respectively, $\eta = P_0/P_{\text{cr}} \cong 50$ and $\rho_0 \cong 37$. The incident azimuthally perturbed transverse amplitude distribution is defined by Eq. (12) with $\varepsilon_q = 0.01$ ($q = 1-4$). The corresponding level of weak azimuthal perturbations is characterized by δ_{pert} from Eq. (13) , $\delta_{\text{pert}} = 0.063$. (a) presents the weakly azimuthally perturbed transverse intensity profile of the incident laser beam. (b) illustrates the transverse structure with the multiple peripheral filaments that have evolved in the process of highly unstable propagation.

B. Scaling to the multipetawatt regime

We now present results that demonstrate that this mechanism of stable channel formation can be extended to powers in the multi-PW regime. Figure 3 illustrates the formation of

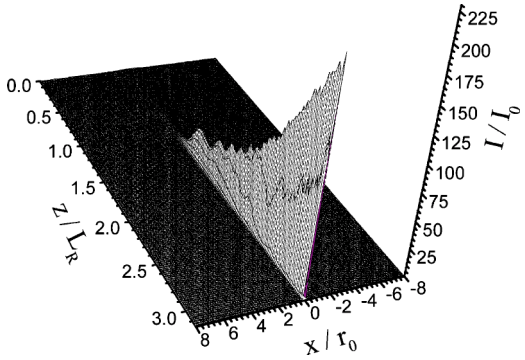

FIG. 2. Dynamics of stable multi-TW channel formation in the initial stage of the propagation with the use of an exponential longitudinal electron density profile defined by $N_{e,0}(z) = N_{e,0}(0)\exp(\alpha z)$ with $N_{e,0}(0) = 1.9 \times 10^{19}$ cm^{-3}, $N_{e,0,\max} = 3.8 \times 10^{20}$ cm^{-3}, and $z_{\max} = 3.16 L_R$ ($\alpha = 0.949$). All other laser pulse parameters are the same as in the previous case depicted in Fig. 1: $\lambda = 248$ nm, $P_0 = 39$ TW, $r_0 = 10$ μm, and $I_0 = 1.2 \times 10^{19}$ W/cm^2. The incident azimuthally perturbed transverse intensity profile is the same as the distribution shown in Fig. 1(a) with $\varepsilon_q \equiv 0.01$ ($q = 1-4$) and $\delta_{\text{pert}} = 0.063$ [see Eqs. (12) and (13)]. The development of a stable channel is presented in the (x,z) plane, where z is the axis of propagation and x is one of the transverse coordinates.

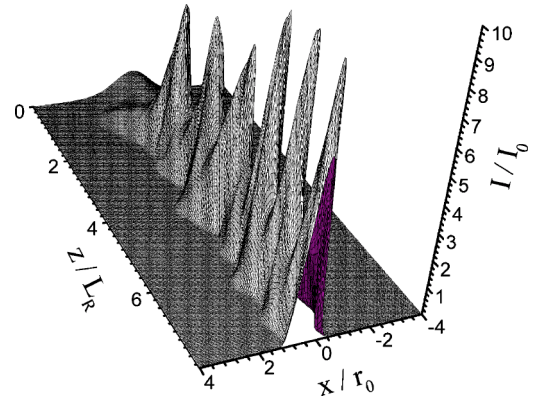

FIG. 4. Dynamics of stable multi-PW relativistic channel formation in the initial stage of propagation with the use of a longitudinal electron density profile defined by Eq. (14) with $N_{e,0}(0) = 5 \times 10^{19}$ cm^{-3}, $N_{e,0,\max} = 3.8 \times 10^{20}$ cm^{-3}, and $z_{\text{exp},2} = 2.96 L_R$. The laser pulse parameters are identical to the case illustrated in Fig. 3: $\lambda = 248$ nm, $P_0 = 7.8$ PW, $r_0 = 2$ μm, and $I_0 = 6.2 \times 10^{22}$ W/cm^2. The incident azimuthally perturbed transverse amplitude distribution is defined by Eq. (12) with $\varepsilon_q \equiv 0.01$ ($q = 1-4$) and the corresponding level of azimuthal perturbation is $\delta_{\text{pert}} = 0.063$ [see Eq. (13)]. The power trapped in the stable relativistic multi-PW laser channel is in the range of 10^4 critical powers.

a stable multi-PW relativistic laser channel. A longitudinal gradient in the electron density profile was initially used to dynamically guide the system to the corresponding eigenmode, as shown above in the terawatt example. The principal laser and plasma parameters in this case are $\lambda = 248$ nm, $P_0 = 7.8$ PW, $r_0 = 2$ μm, $I_0 = 6.2 \times 10^{22}$ W/cm^2, $\varepsilon_q \equiv 0.01$ ($q = 1-4$), $\delta_{\text{pert}} = 0.063$, $N_{e,0}(0) = 5.0 \times 10^{19}$ cm^{-3}, $N_{e,0,\max} = 3.8 \times 10^{20}$ cm^{-3}, and $z_{\max} = 3.95 L_R$. The initial power of $P_0 = 7.8$ PW corresponds to $\eta = 10^4$. Significantly, the power trapped in the stable channel P_{ch} is comparable to P_0; the losses sustained during the formation of the channel are small. Although the longitudinal profile of the electron density utilized had an exponential shape defined by $N_{e,0}(z) = N_{e,0}(0)\exp(\alpha z)$ with $\alpha = 0.514$, additional studies have demonstrated that, for the laser pulse and plasma parameters corresponding to Fig. 3, stability of the propagation can be established with a range of shapes of the electron density profile. Insensitivity to the specific form of the electron density is demonstrated by the results presented in Fig. 4 which shows the development of stable channeled propagation with an electron density profile defined by

$$N_{e,0}(z) = N_{e,0}(0)\{N_{e,0,\max}/N_{e,0}(0) - [N_{e,0,\max}/N_{e,0}(0) - 1] \times \exp[-(z/z_{\text{exp},2})^2]\}, \quad (14)$$

in which $N_{e,0}(0) = 5.0 \times 10^{19}$ cm^{-3}, $N_{e,0,\max}/N_{e,0}(0) = 7.6$, and $z_{\text{exp},2} = 2.96 L_R$. Otherwise, the remaining laser and plasma parameters are identical to those presented in Fig. 3. The stable multi-PW relativistic laser channels presented in Figs. 3 and 4 contain a power on the order of $10^4 P_{\text{cr}}$.

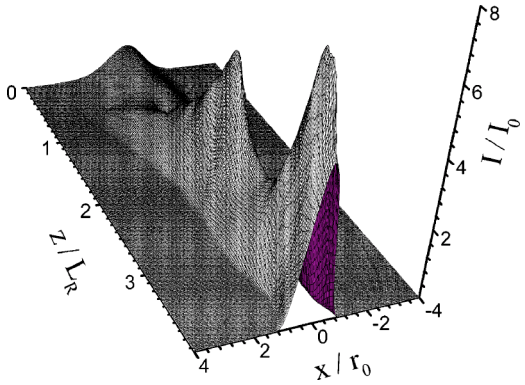

FIG. 3. Dynamics of stable multi-PW channel formation in the initial stage of propagation with the use of an exponential longitudinal electron density profile defined by $N_{e,0}(z) = N_{e,0}(0)\exp(\alpha z)$ with $N_{e,0}(0) = 5 \times 10^{19}$ cm^{-3}, $N_{e,0,\max} = 3.8 \times 10^{20}$ cm^{-3}, and $z_{\max} = 3.95 L_R$ ($\alpha = 0.514$). The laser pulse parameters are $\lambda = 248$ nm, $P_0 = 7.8$ PW, $r_0 = 2$ μm, and $I_0 = 6.2 \times 10^{22}$ W/cm^2. The incident azimuthally perturbed transverse amplitude distribution is defined by Eq. (12) with $\varepsilon_q \equiv 0.01$ ($q = 1-4$) and the corresponding level of azimuthal perturbation is $\delta_{\text{pert}} = 0.063$ [see Eq. (13)]. The power trapped in the stable relativistic multi-PW laser channel is in the range of 10^4 critical powers.

The calculations also indicate that the result shown in Fig. 4 does not represent a physical limit for the conduction of power. The successful establishment of a stable multi-PW relativistic channel with a power exceeding $10^4 P_{\text{cr}}$ is presented in Fig. 5. The chief laser and plasma parameters in this example are $\lambda = 248$ nm, $P_0 = 9$ PW, $r_0 = 5$ μm, $I_0 = 1.1 \times 10^{22}$ W/cm^2, $\varepsilon_q \equiv 0.01$ ($q = 1-4$), $\delta_{\text{pert}} = 0.063$, $N_{e,0}(0) = 7.6 \times 10^{18}$ cm^{-3}, $N_{e,0,\max} = 3.8 \times 10^{20}$ cm^{-3}, and $z_{\max} = 2.37 L_R$. The longitudinal profile of the electron density at the initial stage of the channel formation had an exponential shape defined by $N_{e,0}(z) = N_{e,0}(0)\exp(\alpha z)$ with $\alpha = 1.65$. The transverse profile of the incident laser beam and transverse

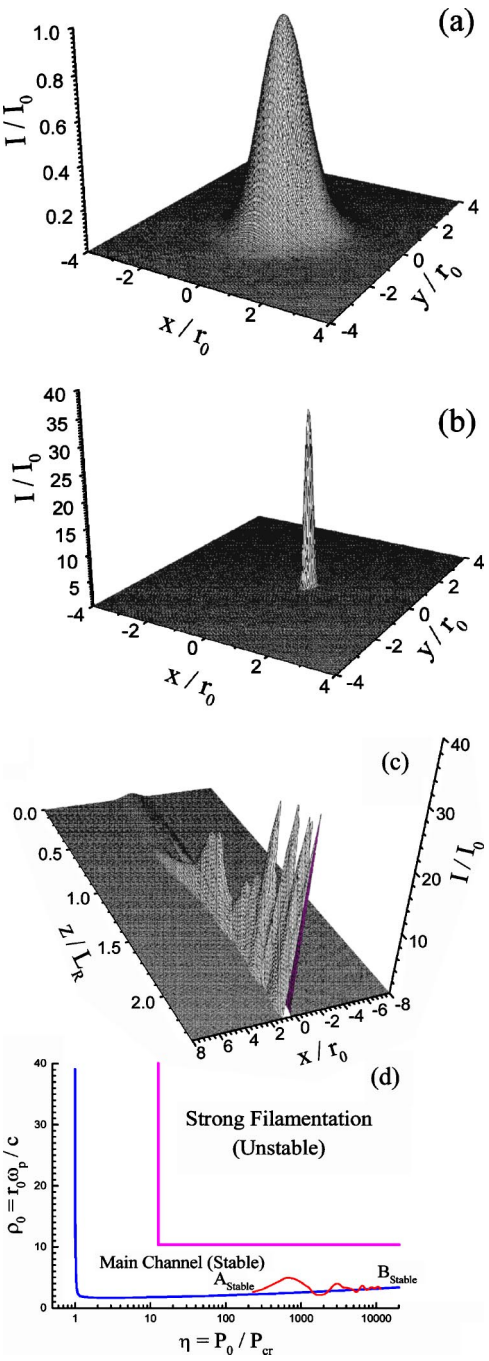

FIG. 5. Stable multi-PW relativistic channel formation in the initial stage of propagation with the use of an exponential longitudinal electron density profile defined by $N_{e,0}(z)=N_{e,0}(0)\exp(\alpha z)$ with $N_{e,0}(0)=1.9\times10^{19}$ cm^{-3}, $N_{e,0,\max}=3.8\times10^{20}$ cm^{-3}, and $z_{\max}=2.37L_R$ ($\alpha=1.65$). The laser pulse parameters are $\lambda=248$ nm, $P_0=9$ PW, $r_0=5$ μm, and $I_0=1.1\times10^{22}$ W/cm^2. The incident azimuthally perturbed transverse amplitude distribution is defined by Eq. (12) with $\varepsilon_q\equiv0.01$ ($q=1-4$) and the corresponding level of azimuthal perturbation is $\delta_{\text{pert}}=0.063$ [see Eq. (13)]. (a) shows the incident azimuthally perturbed transverse intensity profile. The transverse profile of the evolved stable multi-PW relativistic channel is presented in (b). (c) illustrates the dynamics of stable channel formation in the (x,z) plane, where z is the axis of propagation and x is one of the transverse coordinates. The trajectory (solid curve) of stable channel development in the (η,ρ_0) plane [see Eq. (1)] is depicted in (d). The dotted lines represent the boundary between the zone of stable relativistic and ponderomotive self-channeling resulting in the formation of the main powerful channel and the zone of highly unstable self-channeling, which leads to strong filamentation of the laser beam. The dashed curve illustrates the normalized radius of the channel eigenmode $\rho_{e,0}$ defined by Eq. (4) as a function of normalized power η. The initial point of the self-channeling trajectory A_{stable} corresponds to the (η,ρ_0) parameters of the incident laser beam, and the final point of the trajectory B_{stable} illustrates the values of the (η,ρ_0) parameters for the evolved stable ultrapowerful relativistic channel. The power conducted by the stable multi-PW channel exceeds 10^4 critical powers. The peak channel intensity is in the range of 10^{23} W/cm^2.

profile of the stably evolved multi-PW channel are presented in Figs. 5(a) and 5(b), respectively. Figure 5(c) illustrates the dynamics of the process of stable channel formation. The trajectory of the dynamical evolution of the stable propagation, in the plane of dimensionless parameters (η,ρ_0) [see Eq. (1)], is presented in Fig. 5(d). The initial point of the self-channeling trajectory A_{stable} corresponds to the (η,ρ_0) parameters of the incident laser beam and the final point of the trajectory B_{stable} illustrates the values of the (η,ρ_0) parameters for the evolved stable ultrapowerful relativistic channel. It is evident from the position of point B_{stable} that the stable multi-PW relativistic channel depicted in Fig. 5(b) contains more than 10^4 critical powers. Note that the peak intensity in the channel exceeds 10^{23} W/cm^2 under these conditions.

These numerical experiments demonstrate that a two-step approach, which involves an initial phase of propagation through a longitudinal electron density profile, results in stable multi-PW relativistic channel formation, even in the case of a severely distorted incident laser beam that possesses a relatively large initial beam radius. This test of robustness demonstrates that the development of an unstable configuration can be dynamically entirely eliminated, even under very unfavorable conditions of the incident pulse. Figure 6 illustrates a pertinent example supporting this conclusion. The principal laser and plasma parameters in this case

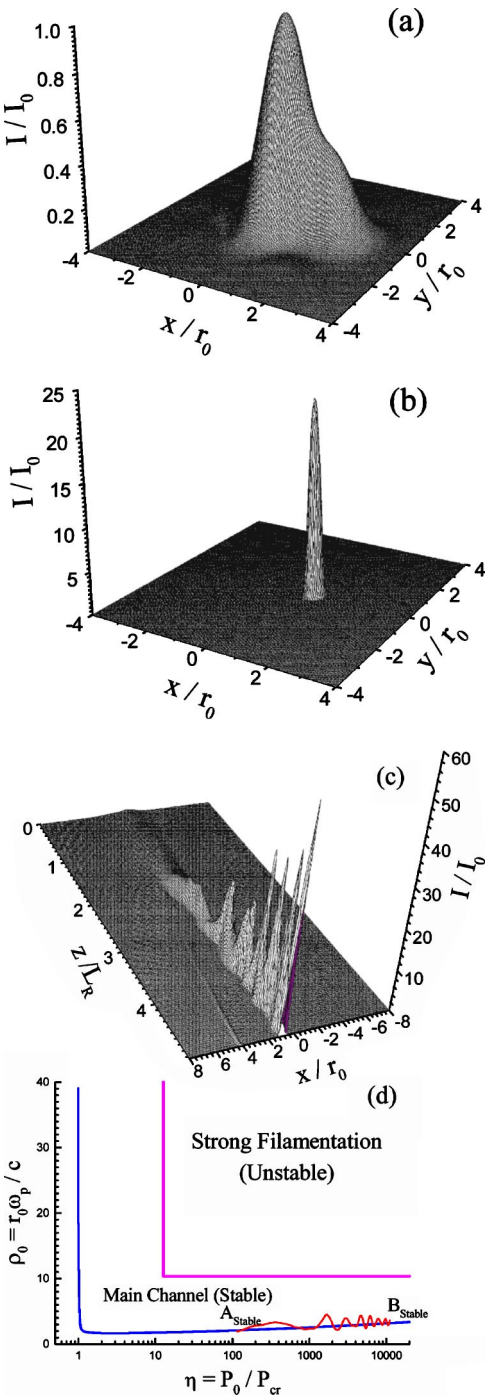

FIG. 6. Stable relativistic channel formation in the case of a severely azimuthally aberrated incident multi-PW laser beam having a relatively large initial beam radius. The exponential longitudinal electron density profile is defined by $N_{e,0}(z) = N_{e,0}(0)\exp(\alpha z)$ with $N_{e,0}(0) = 9.5 \times 10^{17}$ cm^{-3}, $N_{e,0,\max} = 3.8 \times 10^{20}$ cm^{-3}, and $z_{\max} = 4.93 L_R$ ($\alpha = 1.21$). The laser pulse parameters are $\lambda = 248$ nm, $P_0 = 9$ PW, $r_0 = 5$ μm, and $I_0 = 1.0 \times 10^{22}$ W/cm^2. The severely distorted incident transverse amplitude distribution is defined by Eq. (12) with $\varepsilon_q \equiv 0.05$ ($q = 1-4$) and the corresponding level of azimuthal perturbation is $\delta_{\text{pert}} = 0.393$ [see Eq. (13)]. The strongly azimuthally perturbed transverse intensity profile of the incident laser beam is presented in (a). The transverse profile of the evolved stable multi-PW relativistic channel is presented in (b). (c) illustrates in the (x,z) plane the dynamics of the propagation.. The trajectory (solid curve) of stable channel development in the (η, ρ_0) plane [see Eq. (1)] is depicted in (d). The dotted lines represent the boundary between the zone of stable relativistic and ponderomotive self-channeling resulting in the formation of the main powerful channel and the zone of highly unstable self-channeling, which leads to strong filamentation of the laser beam. The dashed curve illustrates the normalized radius of the channel eigenmode $\rho_{e,0}$ defined by Eq. (4) as a function of normalized power η. The initial point of the self-channeling trajectory A_{stable} corresponds to the (η, ρ_0) parameters of the incident laser beam, and the final point of the trajectory B_{stable} illustrates the values of the (η, ρ_0) parameters for the evolved stable ultrapowerful relativistic channel. The power conducted by the channel exceeds 10^4 critical powers and the peak channel intensity is in the range of 10^{23} W/cm^2.

are $\lambda = 248$ nm, $P_0 = 9$ PW, $r_0 = 5$ μm, $I_0 = 1.0 \times 10^{22}$ W/cm^2, $\varepsilon_q \equiv 0.05$ ($q = 1-4$), $\delta_{\text{pert}} = 0.393$, $N_{e,0}(0) = 9.5 \times 10^{17}$ cm^{-3}, $N_{e,0,\max} = 3.8 \times 10^{20}$ cm^{-3}, and $z_{\max} = 4.93 L_R$. The longitudinal profile of the electron density at the initial stage of the relativistic and ponderomotive self-channeling had an exponential shape defined by $N_{e,0}(z) = N_{e,0}(0)\exp(\alpha z)$ with $\alpha = 1.21$. The strongly azimuthally perturbed transverse intensity profile of the incident laser beam is presented in Fig. 6(a). The transverse profile of the evolved stable multi-PW relativistic channel is illustrated in Fig. 6(b). Figure 6(c) demonstrates the dynamics of the stable channel formation in this case, namely, the production of a single channel from a severely azimuthally aberrated incident multi-PW laser beam with a relatively large initial beam radius. Without the dynamics associated with the electron density gradient, this incident pulse would have undergone explosive filamentation. The trajectory of evolution of the stable propagation, in the plane of dimensionless parameters (η, ρ_0) [see Eq. (1)], is presented in Fig. 6(d). It is evident from the position of point B_{stable} that the stable multi-PW relativistic channel pictured in Fig. 6(b) contains more than $10^4 P_{\text{cr}}$.

IV. DISCUSSION OF FINDINGS

The numerical studies performed have demonstrated the exceptional robustness of the control of the channel stability

with the use of an initial buffer zone that involves an appropriate gradient in the electron density profile. Stable channel formation and propagation were preserved under circumstances involving a triplet of extreme physical conditions, all canonically unfavorable to stable behavior. They are (1) an ultrahigh incident power ($P_0/P_{cr}>10^4$), (2) a large mismatch between the radius of the incident beam and the radius of the eigenmode of the relativistic channel ($r_0/r_{ch}>10$), and (3) a high level of azimuthal perturbation in the incident transverse intensity profile ($d_{pert}\sim 0.4$). It is equally important to note that the length of the initial stage of channel formation, in which a single stable ultrapowerful relativistic channel develops, can be relatively short, on the order of the Rayleigh range.

The total length of the channeled propagation is limited only by the incident peak power of the laser pulse and the level of energy losses occurring during propagation. The laser energy is trapped in the stable channel as long as the peak power of the pulse exceeds the critical power P_{cr} for the relativistic and ponderomotive mechanism. Obviously, the ability to confine ultrahigh levels of the laser power in stable channels clearly offers generously extended distances of confined propagation; power and length scaling travel together.

The results of the numerical simulations presented above indicate that stable relativistic channels can contain more than $10^4 P_{cr}$. In addition to the establishment of stability, the two-stage mechanism, which involves an initial phase of propagation that smoothly controls the transition to the key conditions given by Eq. (11) , namely, $r_0\sim r_{ch}$ or $\rho_0\sim\rho_{e,0}$, also leads to the minimization of the energy losses [16] associated with the channel formation. Thus, the two-stage concept of self-channeling automatically provides both energy optimization and robust stability.

The optimization and stability control of relativistic and ponderomotive self-channeling have been demonstrated for a wide range of parameters characterizing the gradient in the electron density profile at the initial stage of the self-channeling (see Figs. 2–6). In all cases studied, a single stable ultrapowerful relativistic channel containing a substantial fraction of incident power was formed. The principal feature that distinguishes the cases considered through the specific values of the parameters characterizing the electron density gradient is the stabilization length. We define this parameter as the distance in the z direction at which the beam transverse intensity profile stabilizes near one of z-independent eigenmode distributions. The typical characteristics of the behavior of this adjustment in the transverse profile of the beam are presented in Figs. 1(a) and 1(b), in the case of unstable self-channeling, and in Figs. 5(a), 5(b), 6(a), and 6(b), under conditions for which a stable ultrapowerful relativistic channel is formed.

Experimental verification of the control of channel stability, using the initial buffer zone with a gradient in the electron density, has been previously presented in Ref. [17]. The observed bifurcation mode of relativistic self-channeling, which involved the splitting of the beam into two powerful filaments, was experimentally converted into a stable mode of propagation by shifting the incident laser focal plane from the central high density region back to the front edge of the gas column, a zone characterized by a lower incident electron density and a sharply rising electron density profile. We note additionally that the two-stage method of self-channeling examined in the present paper, which optimizes both the power compression and the stability, can be applied generally to mechanisms of self-channeling that possess a saturation in the nonlinearity.

One of the important applications of the stable relativistic self-channeling is the efficient generation of ultrabright multi-keV coherent x-ray radiation. Recent experimental observations [20,21] have demonstrated the unique features of the ultrabright $\sim$4.5 keV coherent Xe(L) x-ray emission from Xe clusters irradiated in a stable relativistic channel. This multi-keV x-ray source has the brightness necessary to be a key component of biological microimaging technology applicable to high spatial resolution studies of living matter.

V. CONCLUSIONS

The detailed study of the transverse stability of the mechanism of relativistic and ponderomotive self-channeling has demonstrated that a two-stage process of self-channeling, with the initial phase involving an appropriate gradient in the electron density profile, results in the stable formation of multi-PW relativistic channels in underdense plasmas with a power exceeding 10^4 critical powers and peak channel intensity in the 10^{23} W/cm^2 range at 248 nm. A chief implication of this combination of high power and control is the ability to produce a beam technology with an areal energy density of $\sim 10^9$ J/cm^2 that can propagate for distances many orders of magnitude greater than a Rayleigh length. We note that stable relativistic and ponderomotive self-channeling of intense uv pulses in underdense plasma, producing channels exceeding 100 Rayleigh lengths, has been experimentally demonstrated [10].

ACKNOWLEDGMENTS

The authors thank Dr. C. Martin Stickley for his support and encouragement. This work was supported in part by contracts with the Office of Naval Research (N00173-03-1-6015), the Army Research Office (DAAD19-00-1-0486 and DAAD19-03-1-0189), and Sandia National Laboratories (1629, 17733, 11141, and 25205). Sandia is a multiprogram laboratory operated by the Sandia Corporation, a Lockheed Martin Company, for the United States Department of Energy under Contract No. DE-AC04-94AL85000.

[1] G. A. Askaryan, Zh. Eksp. Teor. Fiz. **42**, 1567 (1962) [Sov. Phys. JETP **15**, 1088 (1962)].
[2] R. Y. Chiao, E. Garmire, and C. H. Townes, Phys. Rev. Lett. **13**, 479 (1964).
[3] P. L. Kelley, Phys. Rev. Lett. **15**, 1005 (1965).
[4] H. A. Haus, Phys. Lett. **8**, 128 (1966).
[5] A. G. Litvak, Sov. Phys. JETP **30**, 344 (1969).
[6] C. Max, J. Arons, and A. B. Langdon, Phys. Rev. Lett. **33**, 209 (1974).
[7] G. Z. Sun, E. Ott, Y. C. Lee, and P. Guzdar, Phys. Fluids **30**, 526 (1987).
[8] A. B. Borisov, A. V. Borovskiy, O. B. Shiryaev, V. V. Korobkin, A. M. Prokhorov, J. C. Solem, T. S. Luk, K. Boyer, and C. K. Rhodes, Phys. Rev. A **45**, 5830 (1992).
[9] A. B. Borisov, A. V. Borovskiy, V. V. Korobkin, A. M. Prokhorov, O. B. Shiryaev, X. M. Shi, T. S. Luk, A. McPherson, J. C. Solem, K. Boyer, and C. K. Rhodes, Phys. Rev. Lett. **68**, 2309 (1992).
[10] A. B. Borisov, X. Shi, V. B. Karpov, V. V. Korobkin, J. C. Solem, O. B. Shiryaev, A. McPherson, K. Boyer, and C. K. Rhodes, J. Opt. Soc. Am. B **11**, 1941 (1994).
[11] V. I. Bespalov and V I. Talanov, Zh. Eksp. Teor. Fiz. Pis'ma Red. **3**, 471 (1966) [JETP Lett. **3**, 307 (1966)].
[12] A. J. Campillo, S. L. Shapiro, and B. R. Suydam, Appl. Phys. Lett. **23**, 628 (1973).
[13] A. J. Campillo, S. L. Shapiro, and B. R. Suydam, Appl. Phys. Lett. **24**, 178 (1974).
[14] A. B. Borisov, O. B. Shiryaev, A. McPherson, K. Boyer, and C. K. Rhodes, Plasma Phys. Controlled Fusion **37**, 56 (1995).
[15] A. B. Borisov, J. W. Longworth, K. Boyer, and C. K. Rhodes, Proc. Natl. Acad. Sci. U.S.A. **95**, 7854 (1998).
[16] A. B. Borisov, S. Cameron, Y. Dai, J. Davis, T. Nelson, W. A. Schroeder, J. W. Longworth, K. Boyer, and C. K. Rhodes, J. Phys. B **32**, 3511 (1999).
[17] A. B. Borisov, S. Cameron, T. S. Luk, T. R. Nelson, A. J. Van Tassle, J. Santoro, W. A. Schroeder, Y. Dai, J. W. Longworth, K. Boyer, and C. K. Rhodes, J. Phys. B **34**, 2167 (2001).
[18] T. Esirkepov, M. Borghesi, S. V. Bulanov, G. Mourou, and T. Tajima, Phys. Rev. Lett. **92**, 175003 (2004).
[19] A. Pukhov, Rep. Prog. Phys. **66**, 47 (2003).
[20] A. B. Borisov, X. Song, F. Frigeni, Y. Koshman, Y. Dai, K. Boyer, and C. K. Rhodes, J. Phys. B **36**, 3433 (2003).
[21] A. B. Borisov, J. Davis, X. Song, Y. Koshman, Y. Dai, K. Boyer, and C. K. Rhodes, J. Phys. B **36**, L285 (2003).